Proceedings of the ASME 2023 42nd International Conference on Ocean, Offshore and Arctic Engineering
OMAE2023
June 11-16, 2023, Melbourne, Australia

OMAE2023-100822

LIDAR-ASSISTED FEEDFORWARD PITCH CONTROL OF 15 MW FLOATING OFFSHORE WIND TURBINES

A. J. Russell[1], M. Collu[2], A. McDonald[3], P. R. Thies[4], A. Mortimer[5], A. R. Quayle[6]

[1]IDCORE, University of Edinburgh, King's Buildings, W Mains Rd, Edinburgh, EH9 3JW, UK
[2]University of Strathclyde, 16 Richmond St, Glasgow, G1 1XQ, UK
[3]University of Edinburgh, King's Buildings, W Mains Rd, Edinburgh, EH9 3JW, UK
[4]University of Exeter, Harrison Building, Streatham Campus, N Park Rd, Exeter, EX4 4QF, UK
[5]Wood Group Plc, 319 St Vincent St, Glasgow, G2 5AS, UK
[6]Flotation Energy Ltd, 12 Alva St, Edinburgh, EH2 4QG, UK

ABSTRACT

Nacelle-mounted, forward-facing Light Detection and Ranging (LIDAR) technology is able to measure the wind field as it approaches a wind turbine. Knowledge of the incoming wind can be used for feedforward turbine control, enabling torque, pitch or yaw systems in advance of the wind's impact. This can enhance turbine performance through improved rotor speed regulation and power capture, while reducing structural loads. LIDAR has previously exhibited its most significant benefits for turbine performance when assisting with blade pitch control in above-rated wind speed conditions. The approach to feedforward pitch control implementation in floating offshore wind turbines has to vary for different substructures due to their differing rates of feedback pitch control actuation, as a consequence of modified controller gains required to overcome negative damping. This computational study compares the LIDAR-assisted feedforward pitch control implementation approaches and results of two floating substructures supporting the IEA 15 MW reference turbine: the UMaine VolturnUS-S Semi-Submersible and the WindCrete Spar. Under turbulent wind conditions and by using a LIDAR simulator to capture the incoming wind field, both floating turbine configurations benefitted from LIDAR-assisted feedforward pitch control, through improved rotor speed regulation by up to 42%, reduced loads by up to 27% and platform motions by up to 35%. These performance improvements can lead to reduced component failure rates, maintenance, and, ultimately, reduced lifetime operations and maintenance expenditure.

Keywords: LIDAR, LIDAR-assisted Control, Feedforward Control, Floating Offshore Wind.

1. INTRODUCTION

The offshore wind industry is growing rapidly, accelerated by the need for global decarbonisation amid the rising threats of climate change. Countries worldwide are recognising the need for cheap, renewable energy to reduce their dependence on oil and gas in the wake of rising costs. In the UK, the government has targeted an offshore wind power capacity of 40 GW by 2030 [1], up from 11 GW in 2021. The capacity of floating offshore wind in the UK is targeted at 1 GW by 2030 [1].

Floating offshore wind turbines are able to capture wind power from further distances offshore, where waters are too deep for use of bottom-fixed turbines. Typically, these greater distances offshore are where winds are strongest, leading to the potential for higher capacity factors (the ratio of actual energy output to the theoretical maximum energy output). Within the UK, the offshore wind farm with the highest recorded lifetime capacity factor is Hywind Scotland, a 30 MW floating wind pilot project in the North Sea, at 52.6% [2].

Operations and maintenance (O&M) expenditure accounts for around 30% of the lifetime costs of a bottom-fixed offshore wind farm [3] and O&M costs for floating wind turbines are expected to be even greater due to their (typically) greater distances offshore. Furthermore, due to constraints in their control configurations, floating wind turbines are also subject to greater variations in rotor speed. This can lead to over-speeding, which risks damage to turbine components and shutdowns. It has been reported that the maximum rotational speed of floating wind turbines are up to 30% higher than the rated speed, compared to only 10% in onshore turbines [4]. Methods to improve the productivity and reliability of floating wind turbines are highly desirable in order to reduce the lifetime levelised costs of floating wind energy, through increased power capture and reduced maintenance. One possible route to achieve this is through Light Detection and Ranging (LIDAR)-assisted turbine control.

LIDAR technology is traditionally used during wind resource assessments, through characterisation of the wind conditions at a potential wind farm location. However, LIDAR can also be nacelle-mounted, and when forward-facing, is able to measure the characteristics of the incoming wind field, which can be used for feedforward (FF) turbine control. Feedforward control enables turbines to actuate their torque, pitch or yaw systems in advance of the wind's impact. This is able to enhance turbine performance through improved rotor speed regulation (thereby mitigating over-speeding events common in floating turbines) and power capture, while reducing structural loads. This has the potential to reduce the levelised cost of offshore wind energy, by extending maintenance intervals and the lifetime of wind turbines, as well as to increase power capture.

Traditionally, turbines utilise feedback (FB) control. This feeds back the turbine's outputs to the relevant controller, which, for wind turbines, are dependent upon the wind conditions. In below rated wind speeds, torque control is used to adjust the rotor speed to maintain the optimal tip speed ratio, through control of the generator torque. In above rated wind speeds, blade pitch control is utilised to maintain the rotor speed at its rated speed. Yaw control is undertaken to ensure that the nacelle of the wind turbine is correctly aligned with the wind.

The pitfall of feedback control is that the turbine is reacting to the wind once it has already impacted upon it. LIDAR-assisted control can overcome this through inclusion of a feedforward control loop (in combination with the feedback control loop), where the incoming disturbance (the wind speed) is measured in advance of it impacting upon the turbine. Knowledge of the incoming disturbance is then used to formulate control commands that can be used by the turbine to pre-emptively prepare for the disturbance. Within the literature, the greatest benefits delivered by LIDAR-assisted control to floating turbine performance and load reductions has been achieved when assisting with blade pitch control in above rated conditions [5][6][7]. An example block diagram for LIDAR-enabled feedforward-feedback (FF-FB) pitch control is given in Figure 1 [8].

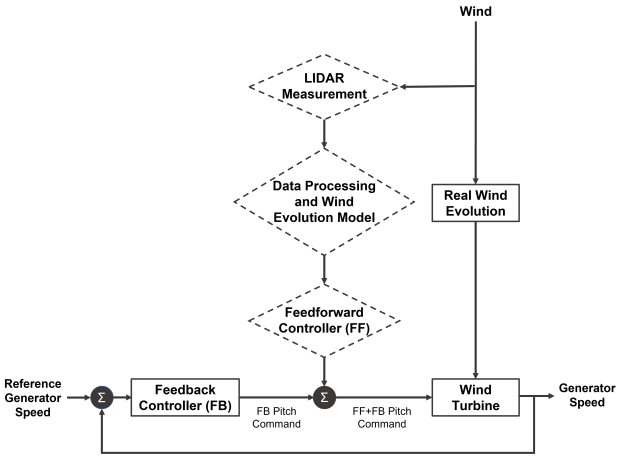

FIGURE 1. LIDAR-enabled FF-FB controller, adapted from [8]. The diamond shaped blocks denote the additional blocks required for the feedforward control, which adds to the existing feedback control.

Previous studies within LIDAR-assisted pitch control have focused on the National Renewable Energy Laboratory (NREL)'s 5 MW reference turbine. Furthermore, for floating turbines, studies have thus far focused on Spar-Buoy [5] and Tension-Leg platforms (TLPs) [6] with the 5 MW reference turbine and Semi-Submersible foundations for a 10 MW turbine model [7]. However, by 2024, turbines of up to 16 MW capacity will be commercially available [9]. Given the commercial direction of increasing wind turbine ratings, it is pertinent to predict the LIDAR-assisted control benefits attainable for these large turbines. Additionally, studies have not yet compared the feedforward control implementation approaches and constraints for different floating substructure topographies. There are likely to be significant differences in the approaches that can be taken due to constraints around the feedback pitch controllers responsiveness, which vary for different substructure designs.

This computational study aims to compare the LIDAR-assisted feedforward pitch control implementation approaches and results of two floating substructures supporting the IEA 15 MW reference turbine: the UMaine VolturnUS-S Semi-Submersible and the WindCrete Spar. The paper aims to showcase the differences in feedforward control implementation for the two substructure designs, as well as the performance improvements and load reductions attainable through implementation of the technology.

2. BACKGROUND

2.1 Floating Turbine Pitch Controller Design

A commonly reported issue for floating turbines is that the pitch controller can become unstable in above rated wind speeds [4][10][11]. This is because the turbines are subject to softer foundation properties, leading to lower natural frequencies and unfavourable coupling between platform motion and blade pitch control [4][11].

The primary issue is that, when using controllers designed for onshore turbines, the floating turbine's pitch controller will adjust pitch angles during the turbine's motion, reducing the thrust when the motion is towards the wind and increasing the thrust when the motion is away from the wind [4]. When the blade pitch control actuation frequency is similar to the floating platform rigid-body pitch oscillation natural frequency, negative damping (oscillations increasing) can occur [4].

Negative damping can lead to serious consequences for turbine performance and increased loadings. Methods for overcoming negative damping include changing the above rated control objective from constant generator torque to constant generator power [4], as well as use of additional sensors [10][11]. However, the most common approach to overcoming negative damping is through re-tuning of the feedback pitch controller [11][12]. This is achieved through modifications (typically reductions) in pitch controller gains, which determine the rate of pitch actuation. The degree of reduction depends on the substructure, which will have differing platform natural frequencies depending on their design. Those that require lower pitch controller gains therefore have slower pitch actuation when compared

to other substructure designs. These rates of pitch actuation are critical when designing the LIDAR enabled feedforward controller, as modifications to the rate of pitch actuation risks re-introducing negative damping. Therefore, different feedforward control implementations are required for different substructure designs.

2.2 Floating Turbine LIDAR-assisted Pitch Control Literature Findings

Previous computational studies in the literature have documented the benefits for floating wind turbine performance attainable through LIDAR-assisted control. These findings provide context for this work and a reference point for which results can be compared to.

Navalkar *et al.* [6] designed a FF-FB pitch controller for a 5 MW turbine on a TLP, assuming perfect LIDAR measurements. Under a wind speed step change, the FF-FB controller reduced extreme speed variation by 45% and the extreme tower displacement by 40% when compared to feedback only control [6]. They also investigated the performance during a turbulent wind field and with a wave height of 5 m. In this case, the standard deviation of the generator speed and loads were reduced by 44% and 24%, respectively, compared to feedback only control [6].

Schlipf *et al.* [5] simulated the implementation of LIDAR on a 5 MW floating wind turbine on a Spar foundation for collective pitch feedforward control. Tests were first performed assuming perfect wind preview, with results shown in Figure 2. The overshoot of the rotor speed could be reduced by 98.9%, the maximum deviation from the static platform pitch angle by 93.7%, and the maximum tower base fore-aft bending moment by 37.8% compared to the feedback controller [5].

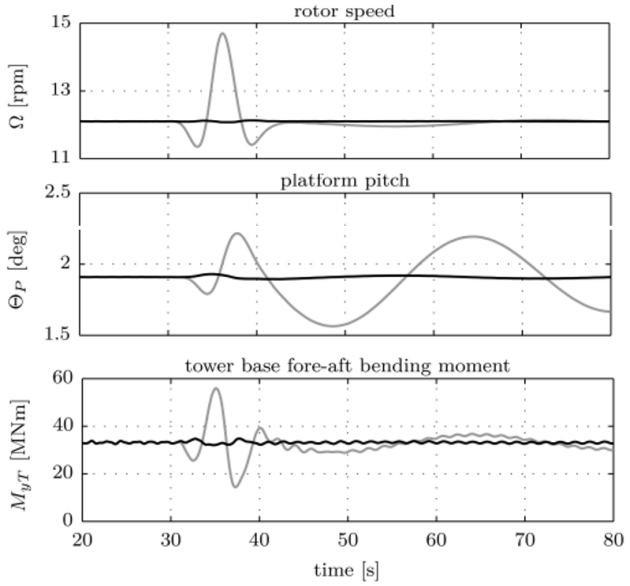

FIGURE 2. Results from [5], comparing performance of the FF-FB (Black) to the baseline FB (Grey) controller with perfect wind preview.

Simulations were then performed using a LIDAR simulator, developed in [13], to scan the wind field used in the numerical simulation. For applicability to floating turbines, the simulator was extended to include platform motions in order to realistically reproduce LIDAR measurements from a floating wind turbine. They reported that a good agreement was found between the rotor-effective wind speed from the wind field and its filtered, time-shifted estimate from the LIDAR (see Figure 3). Even with the more realistic wind preview, the rotor speed variation was still significantly reduced, in addition to the platform motions and the tower base bending moment [5]. Reductions in loads on the tower base of 20% were achieved as well as 7% and 9% reductions on the shaft and blade root loads, respectively.

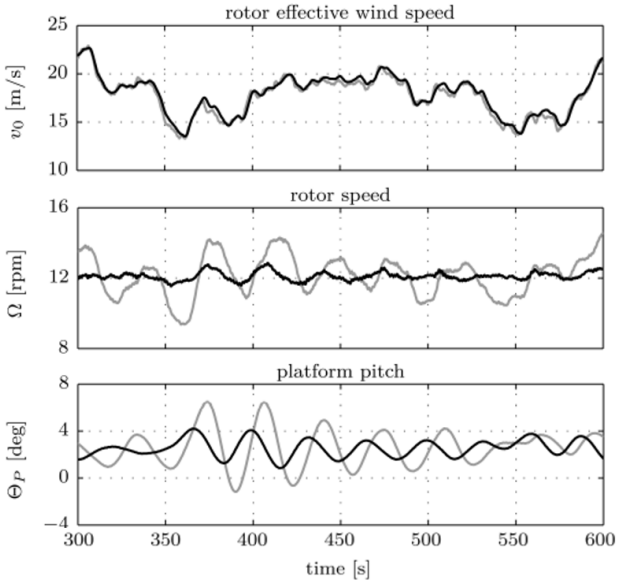

FIGURE 3. Results from [5]. Top: LIDAR captured (Black) vs. Simulated wind speed (Grey). Middle/Bottom: Comparing performance of the FF-FB (Black) to the baseline FB (Grey) controller with realistic wind preview.

3. METHODOLOGY

This section will provide information regarding the software, turbine and substructure models used in performing the simulations. Furthermore, detail will be provided on how the simulations were configured and how feedforward control was implemented.

3.1 OpenFAST, MATLAB & Simulink

The numerical modelling tool employed for this study was NREL's open source Fatigue, Aerodynamics, Structures, and Turbulence (FAST) code. This software is classed as an aero-servo-hydro-elastic tool for the modelling of full nonlinear wind turbine models. It allows for intricate specification of the turbine's design, external environment (wind, wave and current conditions), and the controller design. OpenFAST is the latest iteration of the FAST code and version 3.0 was used for this study [14].

3.1.1 Simulink Interface

Critical to the employment of the designed controller algorithms is OpenFAST's interface with Simulink, a MATLAB-based graphical programming environment. MATLAB/Simulink R2019b edition was used in this study [15]. To enable control via Simulink, this was specified in the ServoDyn (control module) file of OpenFAST.

3.2 Turbine and Substructure Models

3.2.1 Turbine

The turbine studied in this work is the IEA-Wind 15 MW reference turbine, developed between NREL and the Technical University of Denmark (DTU), via the International Energy Agency (IEA), as defined in [16]. The specifications of the reference turbine are given in Table 1.

TABLE 1. Parameters of the IEA-Wind 15 MW reference turbine, from [16].

Parameter	Units	Value
Power rating	MW	15
Turbine class	-	IEC Class 1B
Cut-in wind speed	m/s	3
Rated wind speed	m/s	10.59
Cut-out wind speed	m/s	25
Design tip-speed ratio	-	9.0
Minimum rotor speed	rpm	5.0
Maximum rotor speed	rpm	7.56
Rotor diameter	m	240
Hub height	m	150
Drive train	-	Direct Drive

The turbine rotor operates with a minimum rotational speed of 5 rpm to avoid 3-period (3P) interference with the tower/monopile natural frequencies [16], and reaches a rated rotational speed of 7.55 rpm at 10.59 m/s. The blades begin pitching at the rated wind speed in order to maintain the rotor rotation at its rated speed.

The baseline feedback controller used by the IEA Wind 15 MW reference wind turbine is the NREL Reference OpenSource Controller (ROSCO), as described in [17]. It uses a gain-scheduled feedback proportional-integral (PI) pitch controller in above-rated wind speed conditions. The ROSCO controller is typically packaged into a dynamic link library (.dll) file to be called by the ServoDyn file. However, it has been translated into a Simulink model [18], which was further developed in this study for the implementation of feedforward measurements from a LIDAR simulator.

3.2.2 Substructures

The floating substructure models utilised for this work were the University of Maine's (UMaine) VolturnUS-S Semi-Submersible [19] and the WindCrete Spar, developed by the EU Horizon 2020 project COREWIND [20] . Both floaters are designed to support the IEA 15 MW reference wind turbine. Key specifications for the substructures are shown in Table 2 and the floating turbines are depicted in Figure 4.

TABLE 2. Parameters of the two substructure models, from [19] and [20]. Both are modelled in a water depth of 200 metres.

Parameter	Units	VolturnUS-S	WindCrete
Hub Height	m	150	135
Material	-	Steel	Concrete
Draft	m	20	155
Mass (inc. Ballast)	kg	17,839	39,805
Mooring System	-	3-line Catenary	3-line Catenary

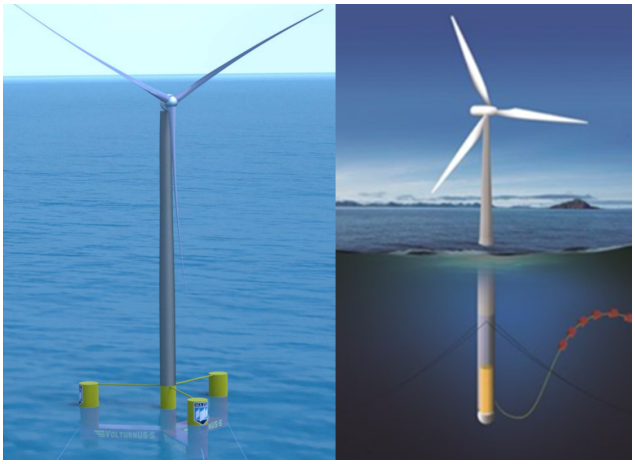

FIGURE 4. The UMaine VolturnUS-S (left) and WindCrete Spar (right) platforms designed to support the IEA-15-240 RWT system, from [19] and [20].

3.3 Model Set-Up and Validation

To ensure that any results are valid, steady state reference values for different parameters must be obtained that match those reported in the reference documentation [16]. The OpenFAST model of the bottom-fixed turbine was simulated at each individual wind speed integer with still water until steady state was achieved. The results of the model validation are shown in Figure 8 within Section 4.1.

3.3.1 Fixed to Floating Transfer - Controller Detuning

To enable transfer to floating turbines, changes have to be made to the PI gain schedule of the turbine's pitch controller. This is because, in above rated wind speeds, unfavourable coupling occurs between the pitch controller and the platform motion. To overcome this, the pitch controller's PI gains can be reduced, which brings the blade pitch actuation frequency out of the bandwidth of that of the platform pitching frequency. The corrected proportional and integral gains for the blade pitch controller of each substructure were defined by the designers within their respective ROSCO controller input files [19][20]. For the VolturnUS-S, the pitch controller was tuned by modifying the target pitch controller damping ratio and natural frequency to 1.0 and 0.2 radians per second (rad/s), respectively [19]. The WindCrete Spar's pitch controller was tuned using the Ziegler-Nichols method [21], whereby the controller gains were tuned at one wind speed before the ratio of reduction was applied to the other points in the gain schedule [20].

3.3.2 Comparison of Turbine-Substructure Baseline Pitch Behaviour

To understand the required approach to the feedforward implementation for the different substructures, it was important to assess their behaviour in terms of their respective rates of pitch variation. The responsiveness of the feedback control system is dependent upon the proportional and integral gains of the PI controller. Through comparison of the gain schedules of both substructures' ROSCO controller input files, the average proportional and integral

controller gains for the Volturn US-S were found to be 4.17 times and 21.9 times greater than those of the WindCrete Spar, respectively. This leads to a significantly more responsive feedback pitch controller, as reflected in the time series of pitch variation under a turbulent wind field, shown in Figure 5.

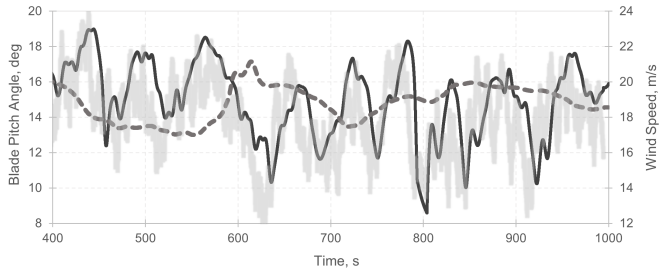

FIGURE 5. Time series plot comparing the blade pitch of the VolturnUS-S (Black, solid) and the WindCrete Spar (Dark Grey, dashed) under a turbulent wind field (Light Grey, faded).

As can be seen in Figure 5, the VolturnUS-S' feedback pitch controller is significantly more responsive than that of the WindCrete Spar and is better able to respond to variations in wind speed. Consideration of the rate of pitch change is paramount to the design of the feedforward controller because significant changes to the pitching frequency risks the re-introduction of detrimental negative damping. Therefore, different feedforward control implementations were required for the different substructures.

3.4 Feedforward Control Implementation

This section will detail how the feedforward control was implemented for each substructure to allow for a feedforward update to the blade pitch controller in above-rated conditions.

3.4.1 Feedforward Control Implementation - VolturnUS-S

The feedforward implementation for the VolturnUS-S is illustrated in Figure 6.

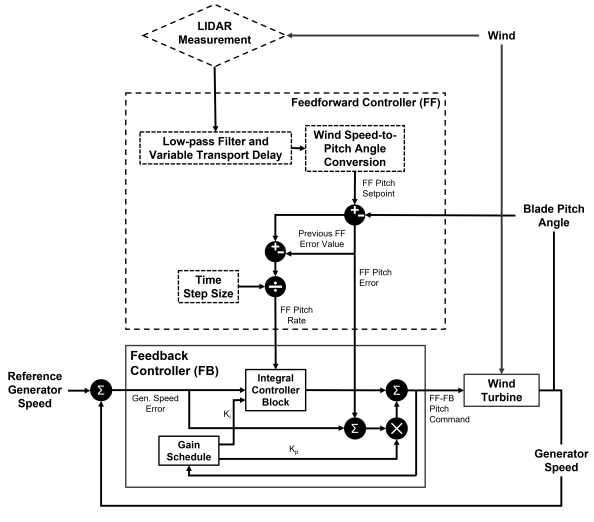

FIGURE 6. Flowchart illustrating the feedforward control implementation into the VolturnUS-S.

Given the responsive nature of the VolutrnUS-S' pitch actuation as a result of its (comparatively) high feedback pitch controller gains, it was possible to implement a feedforward update directly to the feedback pitch controller, as depicted in Figure 6. The LIDAR measurement was fed to a look-up table, which determined the required pitch angle for the measured incoming wind speed. The error between this value and the actual, current blade pitch angle was then computed. This error was used in two ways. Firstly, it was combined with the feedback generator speed error, which was then multiplied by the proportional gain of the feedback controller. Concurrently, the difference between the current feedforward error and that computed at the previous time step was calculated and divided by the time-step duration. This rate value was then added to the integral part of the feedback controller. These modifications provided enhancement to the feedback controller by ensuring appropriate blade pitch actuation in preparation for changes in wind speed.

3.4.2 Feedforward Control Implementation - WindCrete

The feedforward implementation for the WindCrete Spar is illustrated in Figure 7.

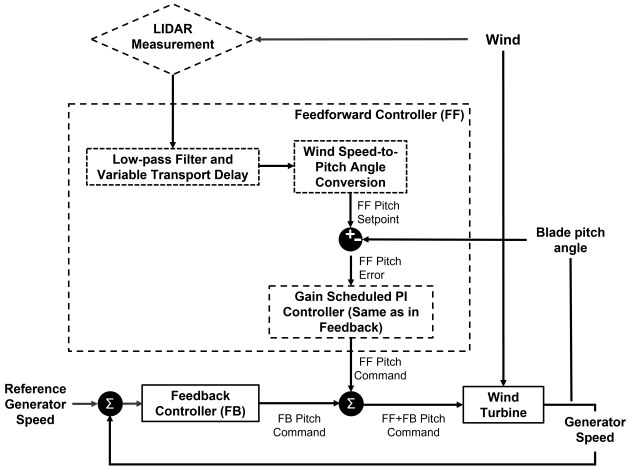

FIGURE 7. Flowchart illustrating the feedforward control implementation into the WindCrete Spar.

As the rate of pitch actuation is slower in the WindCrete Spar than the VolturnUS-S due to lower pitch controller gains, there were more restrictions on the design of the feedforward controller. Significant changes to the pitching rate risked re-introducing negative damping. Therefore, a feedforward pitch command value was combined with the feedback pitch command, as shown in Figure 7, to ensure that the pitching rate was not affected. The LIDAR-measured wind speed-to-pitch angle look up table was again used when computing the feedforward pitch error. The same PI gain scheduled controller used in the feedback controller was then used to determine the feedforward pitch command to be combined with the feedback pitch command. The same PI gain schedule was used because differing gains resulted in significant changes to the rate of pitch actuation, which lead to increased loadings.

3.5 Simulation Configuration

3.5.1 Wind Speed Step Change

Analysis was first performed under a wind speed step change from 13 m/s to 19 m/s. The baseline FB controller performance was compared to that of the FF-FB controller. This experiment was only performed for the VolturnUS-S. Comparison was undertaken through assessment of the standard deviations of the time series results as well as the overshoot that occurs when the step change occurs. The overshoot was calculated by subtracting the steady-state value at 13 m/s from that of the highest value of the overshoot peak. Throughout this study, the percentage difference between the baseline FB and FF-FB control values of standard deviation or overshoot were used to quantify the percentage reductions or increases.

Within the InflowWind simulation file of OpenFAST, the wind speed was configured to step-up at a specified time. In the Simulink model, a step-change block was included and was configured to occur 2 seconds before the change occurs in the OpenFAST model, analogous to a LIDAR device providing the turbine with 2 seconds of preview time.

3.5.2 Turbulent Wind Field

Simulations were then performed under a turbulent wind field for both substructure configurations. The turbulent wind field was created via TurbSim from a configured input file. The average wind speed was specified as 18 m/s, with turbulence intensity (TI) category B. Both substructures were subjected to the same wind field. Both substructures were also subjected to the same irregular wave sea state, with regard to the water depth (200 m), significant wave height (3.06 m) and peak spectral wave period (8.05 s). These conditions fall into design load case (DLC) 1.1, as defined in [22].

3.5.3 LIDAR Simulation

LIDAR simulation was implemented using the LIDAR simulator developed by Schlipf et al. [13] and further enhanced by Guo et al. [23] with blade blockage, LIDAR availability, and wind evolution features. These additional features were not used in this study. The LIDAR simulator is able to measure the incoming wind speed while considering the motions of the LIDAR on the nacelle due to the platform motions and accelerations. Within the simulations, the LIDAR was configured with a single beam measuring at a focal distance of 100 m upstream of the turbine, at a measurement frequency of 4 Hz.

3.5.4 Variable Transport Delay

In order to give the turbine the desired amount of preview time, a variable transport delay was implemented. This was calculated by dividing the focal distance by the LIDAR measured wind speed to determine the total travel time of the wind from the point of measurement to contact with the turbine. This was then reduced by the desired preview time to ensure that the same pitch command preview was provided, regardless of the wind speed. Two seconds of preview time was provided during the simulations.

4. RESULTS

4.1 Model Validation

Figure 8 shows the results of the model validation. The steady state values at each wind speed integer were recorded.

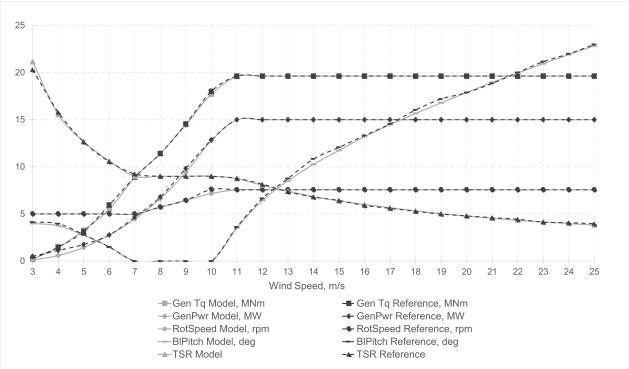

FIGURE 8. Validation of model values to match the reference values reported in [16]. The y-axis dimensions for each parameter corresponds to those specified in the legend.

From Figure 8, all steady state model values match the reference values within +/- 5%. This verification process ensures confidence in the subsequent results.

4.2 Feedforward Implementation - Step Change

Figure 9 shows the results of the wind speed step change simulation.

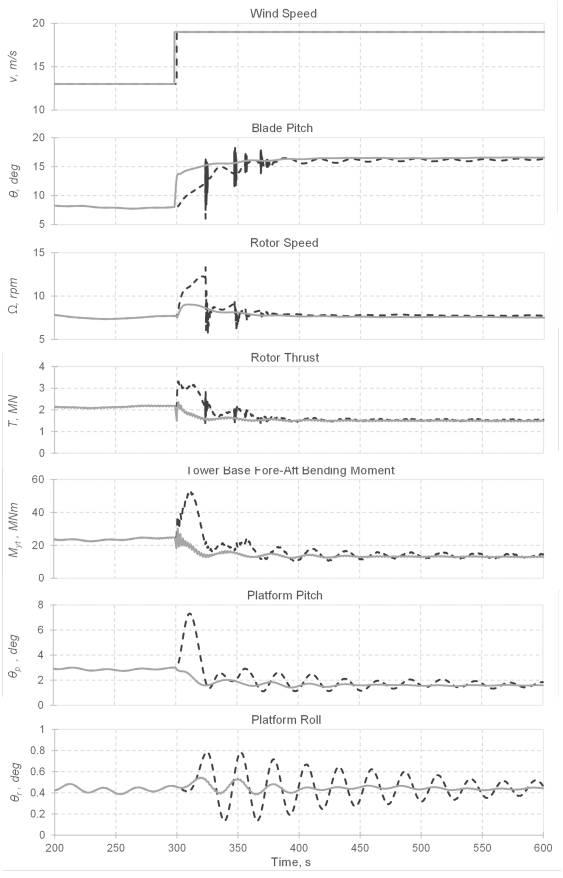

FIGURE 9. Results of FF-FB control performance vs. the baseline FB controller of the Volturn US-S under a wind speed step change. Black, dashed = FB. Grey, solid = FF-FB.

The implementation of feedforward control resulted in significant reductions in the overshoot of important parameters following the wind speed step change. The standard deviations of the parameters were also reduced significantly compared to the baseline feedback controller, including that of the rotor speed by 61%. This is attributed to the blade pitch angle being adjusted in advance of the wind speed change, such that the rotor and blades are prepared for the sudden change in wind speed. A summary of the reductions are shown in Table 3.

TABLE 3. Percentage reductions in standard deviation of turbine parameters through the addition of feedforward control vs. baseline feedback control under a wind speed step change.

Parameter	Overshoot reductions (FF-FB vs. FB)	Standard dev. reductions (FF-FB vs. FB)
Rotor Speed	75%	61%
Rotor Thrust	81%	29%
Tower Base Bending	77%	38%
Platform Pitch	99.8%	45%
Platform Roll	31%	77%

4.3 Feedforward Implementation - Turbulent Wind

4.3.1 LIDAR Measured vs Actual Wind Speed

Figure 10 shows how the filtered, time-shifted rotor effective wind speed obtained from the LIDAR simulator corresponds to the actual wind speed.

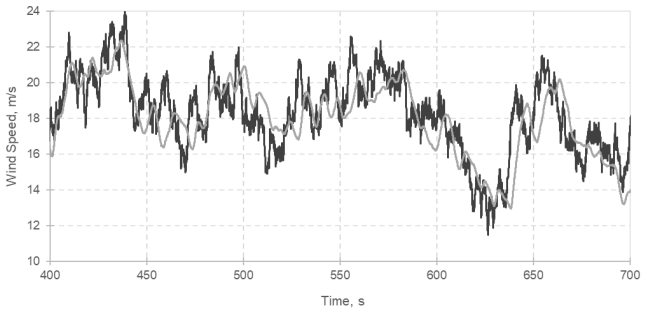

FIGURE 10. Time series plot of the actual wind speed (Dark Grey) to the simulated, time-shifted and filtered LIDAR measured wind speed (Light Grey).

As can be seen from Figure 10, the LIDAR simulator is able to follow the variations in the incoming wind field.

4.3.2 VolturnUS-S Semi-Submersible

This section presents the results for the VolturnUS-S Semi-Submersible beginning with the comparison between the baseline FB controller and the FF-FB controller for turbine performance and loadings (Figures 11 and 12).

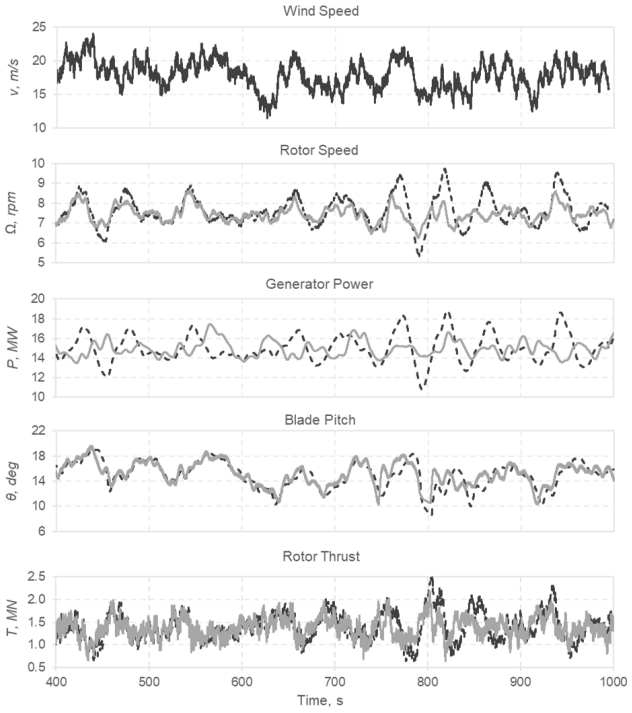

FIGURE 11. Results of FF-FB control vs. the baseline FB controller on the performance of the Volturn US-S under a turbulent wind field. Black, dashed = FB, Grey, solid = FF-FB.

From Figure 11, the feedforward control implementation improved rotor speed and power regulation, with both experiencing a 42% reduction in standard deviation compared to the baseline feedback controller. Additionally, due to the superior pitch rate control enabled by the feedforward controller, the standard deviation of the blade pitch was reduced by 13% compared to the baseline controller. The standard deviation of the rotor thrust was also reduced by 29% compared to the baseline.

The addition of feedforward control also mitigated over-speeding of the rotor. The maximum rotor speed when using the baseline feedback controller was 29% greater than the rated rotor speed. When using the FF-FB controller, the maximum rotor speed was reduced to 16% greater than the rated speed.

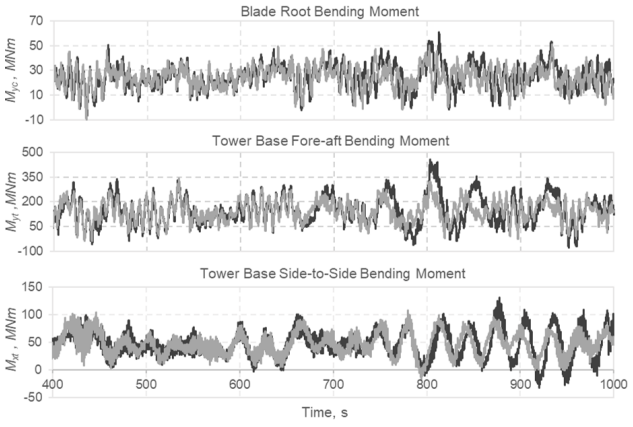

FIGURE 12. Results of FF-FB control vs. the baseline FB controller for loadings on the Volturn US-S under a turbulent wind field. Black = FB. Grey = FF-FB.

As shown in Figure 12, loadings on the tower base and blade root were decreased. Reductions in the standard deviation of the tower base bending moment in both the fore-aft (26%) and side-to-side directions (23%) compared to the baseline feedback controller were recorded. Meanwhile, the blade root bending moment also saw a 14% reduction in standard deviation. The feedforward addition also had positive impacts on platform motions, with reductions in the pitch and roll standard deviations of 35% and 28%, respectively, compared to the feedback controller, as shown in Figure 13 .

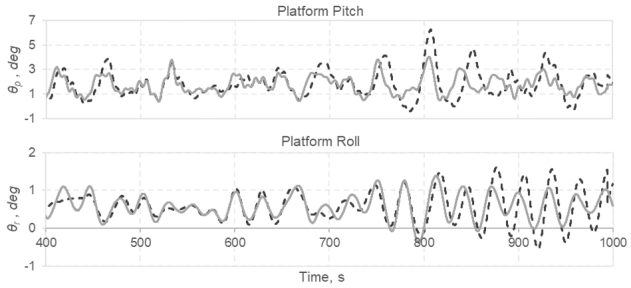

FIGURE 13. Results of FF-FB control vs. the baseline FB controller for motions of the Volturn US-S under a turbulent wind field. Black, dashed = FB. Grey, solid = FF-FB.

4.3.3 WindCrete Spar

This section presents the time series results for the WindCrete Spar, starting with performance parameters (Figure 14).

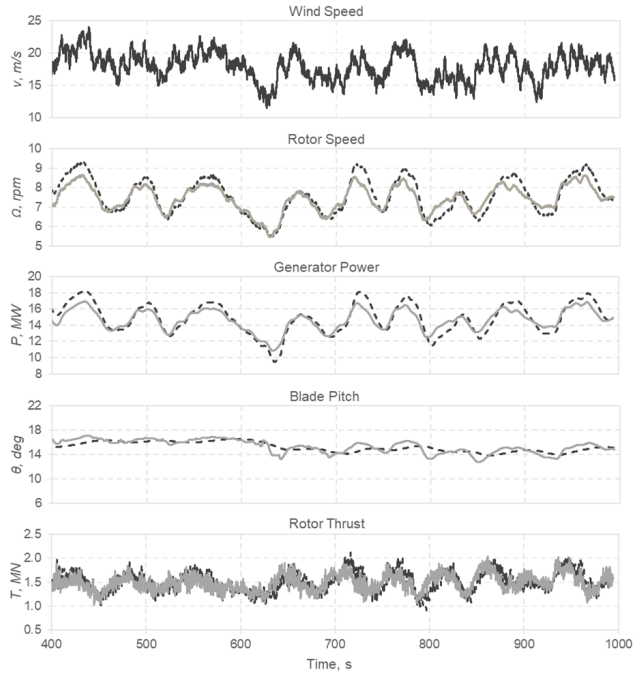

FIGURE 14. Results of FF-FB control vs. the baseline FB controller on the performance of the WindCrete Spar under a turbulent wind field. Black, dashed = FB, Grey, solid = FF-FB.

As seen in Figure 14, the rotor speed, power and thrust all benefited from the feedforward control addition, experiencing reductions of 24%, 24% and 6% in their standard deviations, respectively, compared to the baseline feedback controller. However, the standard deviation in the blade pitch increased by 45% from the baseline, which was expected due to the slow rate of actuation of the baseline feedback controller. The maximum rotor speed when using the baseline feedback controller was 23% greater than the rated rotor speed. When using the FF-FB controller, the maximum rotor speed was reduced to 15% greater than the rated speed.

The FF-FB controller was able to increase the pitch actuation without reintroducing negative damping, as shown by the impacts on the loadings in Figure 15.

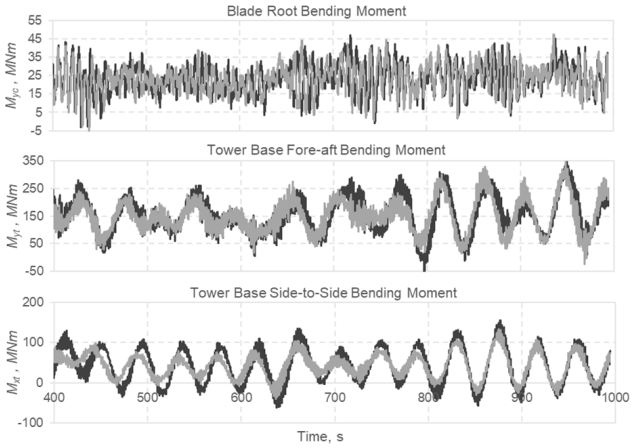

FIGURE 15. Results of FF-FB control vs. the baseline FB controller on the loadings of the WindCrete Spar under a turbulent wind field. Black = FB, Grey, = FF-FB.

The addition of FF control delivered reductions in the standard deviations of the tower base bending moments of 14% and 27% in the fore-aft and side-to-side directions, respectively, compared to the baseline feedback controller.

The WindCrere Spar also benefited from reductions to the standard deviation in the pitch (11%) and roll (29%) motions of the platform when using FF-FB control instead of feedback only control, as shown in Figure 16.

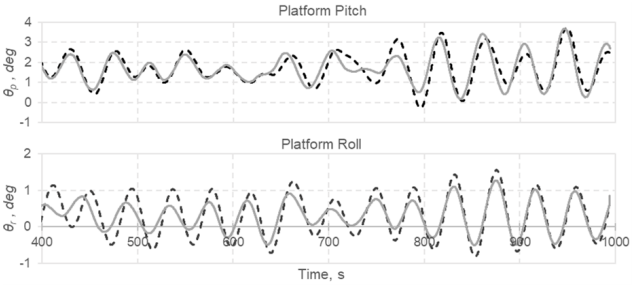

FIGURE 16. Results of FF-FB control vs. the baseline FB controller for motions of the WindCrete Spar under a turbulent wind field. Black, dashed = FB, Grey, solid = FF-FB.

4.3.4 Summary Table

Table 4 gives a summary of the standard deviation reductions (or increases) resulting from the feedforward control additions compared to the baseline feedback control.

TABLE 4. Percentage difference in standard deviation of various parameters through the addition of feedforward control vs. baseline feedback control under a turbulent wind field. A positive value corresponds to a reduction, and a negative value corresponds to an increase.

Parameter	VolturnUS-S Standard dev. reductions (FF-FB vs. FB)	WindCrete Standard dev. reductions (FF-FB vs. FB)
Performance		
Rotor Speed	42%	24%
Generator Power	42%	24%
Blade Pitch	13%	-45%
Rotor Thrust	29%	6%
Bending Moments		
Blade Root	14%	4%
Tower Base Fore-aft	26%	14%
Tower Base Side-to-Side	23%	27%
Platform Motions		
Yaw	0%	6%
Pitch	35%	11%
Roll	28%	29%
Heave	-7%	12%
Sway	-1%	23%
Surge	20%	0%

5. DISCUSSION

The improvements in the parameters shown in Table 4 have been attributed to the superior blade pitch preparation achieved through the addition of FF control, as the pitch is adjusted in advance of the wind speed changes.

The results align with those published in [5], where similar standard deviation reductions of the key parameters were documented, as shown in Figure 3. This work has demonstrated that LIDAR-assisted control can provide performance benefits, loads and motion reductions to large, commercial-scale floating wind turbines with Semi-Submersible or Spar platform configurations.

Overall, the Volturn US-S benefited more from the feedforward control addition than the WindCrete Spar, with superior standard deviation reductions in turbine performance and loading parameters. The VolturnUS-S had fewer restrictions on the changes that could be made due to its capacity for a higher rate of blade pitching. The WindCrete Spar's feedforward controller had to be designed to match the behaviour of the feedback pitch controller to avoid re-introducing negative damping and so there was less scope for changes, which led to less significant improvements. These differences may also be apparent because the VolturnUS-S has an inherently higher dynamic response to wind and waves, leading to more room for improvement for the feedforward-feedback controller. However, the motions of WindCrete Spar benefitted greatly from the feedforward addition, with all degrees of freedom except for surge and yaw seeing a greater than 10% reduction in standard deviation. It has been reported that the Hywind Scotland Spar platforms use an additional floater motion control system to dampen out floater motions by pitching of the blades [24]. The results reported here indicate that LIDAR-assisted control is also able to deliver this benefit.

The addition of LIDAR-assisted control also aided both turbines in mitigating over-speeding of the rotor. The superior rotor speed regulation prevented the turbines from over- and under-powering. Reduced over- and under-speeding results in more consistent power capture and can also prevent shutdown events, thereby increasing lifetime power capture.

5.1 Novelty and Contributions to the Field

The below list gives the aspects of novelty and contributions to the field from this work. To the best of the authors' knowledge at the time of writing, this study is the first to:

- Investigate the performance enhancements and load reductions that can be achieved through LIDAR-assisted feedforward control on a 15 MW floating turbine.
- Study LIDAR-assisted control on a 15 MW Semi-Submersible substructure.
- Compare the differences in feedforward control implementation between different 15 MW substructure designs.

6. CONCLUSIONS

This computational study investigated the implementation of LIDAR-assisted feedforward pitch control into two floating substructures supporting the IEA 15 MW reference turbine: The University of Maine's VolturnUS-S Semi-Submersible and the WindCrete Spar.

When designing the feedforward controllers, special consideration had to be made for the baseline feedback pitch controller's proportional-integral gains, which determine the rate of pitch actuation of the turbine's blades. Through comparison of their respective blade pitch time series under a turbulent wind field, it was found that the VolturnUS-S had a much more responsive feedback pitch controller than the WindCrete Spar. The feedforward controllers had to be designed around the constraints imposed by these differences. For the VolturnUS-S, the feedforward controller was designed to directly interface with the feedback pitch controller's proportional and integral components so that the blade pitch could maintain pace with changes in the turbulent wind field. For the WindCrete Spar, changes had to be more discrete due to the risk of re-introducing negative damping by increasing the pitching rate. Therefore, a feedforward pitch command value was issued and combined with that provided by the feedback controller.

Both substructures benefitted from the addition of feedforward control, with improvements to turbine performance, loadings and platform motion reductions. The VolturnUS-S experienced standard deviation reductions of 42% in the rotor speed and 13% in the blade pitch compared to the baseline feedback controller. 26% and 23% reductions in the tower base fore-aft and side-to-side bending moments, respectively, were also recorded. Platform motions were also reduced in pitch, roll and surge by 35%, 28%, and 20%, respectively.

The standard deviation of WindCrete Spar's rotor speed was decreased by 24% through the addition of LIDAR-assisted control. However, this came at the expense

of increased blade pitching, where the standard deviation increased by 45%. This increase did not lead to a re-introduction of negative damping, as tower base bending moments were reduced by 14% and 27% in the fore-aft and side-to-side directions, respectively. The motions of the WindCrete Spar were also decreased by 29% in pitch, 11% in roll and 23% in sway.

Future work aims to investigate the potential lifetime cost savings achievable through LIDAR-assisted pitch control of floating offshore wind turbines. These cost savings are expected to be achievable through the extension of component lifetimes, reduced downtime and operations and maintenance activities, and increased power capture.

ACKNOWLEDGEMENTS

This work was funded by UK Research and Innovation as part of the EPSRC and NERC Industrial CDT for Offshore Renewable Energy (IDCORE), Grant number EP/S023933/1.

The authors would like to thank David Schlipf and Feng Guo of Flensburg University of Applied Sciences for providing the OpenFAST LIDAR simulator used in this study, as detailed in [23], as well as sharing knowledge of feedforward control modelling in OpenFAST.

REFERENCES

[1] UK Government. New plans to make UK world leader in green energy, 2020. URL: https://www.gov.uk/government/news/new-plans-to-make-uk-world-leader-in-green-energy.

[2] Energy Numbers. UK offshore wind capacity factors, 2022. URL: https://energynumbers.info/uk-offshore-wind-capacity-factors.

[3] I. Dinwoodie et al. Development of a combined operational and strategic decision support model for offshore wind. *Energy Procedia*, 35:157–166, 2013.

[4] T.J. Larsen and T.D. Hanson. A method to avoid negative damped low frequent tower vibrations for a floating, pitch controlled wind turbine. In *Journal of Physics: Conference Series*, volume 75, page 012073. IOP Publishing, 2007.

[5] D. Schlipf et al. Collective pitch feedforward control of floating wind turbines using LIDAR. In *The Twenty-fifth International Ocean and Polar Engineering Conference*. OnePetro, 2015.

[6] S.T. Navalkar et al. Integrating robust LIDAR-based feedforward with feedback control to enhance speed regulation of floating wind turbines. In *2015 American Control Conference (ACC)*, pages 3070–3075. IEEE, 2015.

[7] D. Schlipf, F. Lemmer, and S. Raach. Multi-variable feedforward control for floating wind turbines using LIDAR. In *The 30th International Ocean and Polar Engineering Conference*. OnePetro, 2020.

[8] A. Scholbrock et al. LIDAR-enhanced wind turbine control: Past, present, and future. In *2016 American Control Conference (ACC)*, pages 1399–1406. IEEE, 2016.

[9] Ming Yang Smart Energy. Leading innovation: Mingyang Smart Energy launches MySE 16.0-242, the worlds largest offshore hybrid drive wind turbine, 2021. URL: http://www.myse.com.cn/en/jtxw/info.aspx?itemid=825.

[10] P. Fleming et al. Evaluating methods for control of an offshore floating turbine. In *International Conference on Offshore Mechanics and Arctic Engineering*, volume 45547, page V09BT09A019. American Society of Mechanical Engineers, 2014.

[11] W. Yu et al. Evaluation of control methods for floating offshore wind turbines. In *Journal of Physics: Conference Series*, volume 1104, page 012033. IOP Publishing, 2018.

[12] J. Jonkman. *Dynamics modeling and loads analysis of an offshore floating wind turbine*. University of Colorado, Boulder, 2007.

[13] D. Schlipf et al. Development of a wind turbine LIDAR simulator. University of Stuttgart, 2009.

[14] National Renewable Energy Laboratory (NREL). OpenFAST v3.0.0, 2021. URL: https://github.com/OpenFAST/openfast/tree/v3.0.0.

[15] MathWorks. R2019b at a Glance, 2019. URL: https://uk.mathworks.com/products/new_products/release2019b.html.

[16] E. Gaertner et al. Definition of the IEA wind 15-MegaWatt offshore reference wind turbine tech. rep. Technical report, NREL/TP-5000-75698 National Renewable Energy Laboratory Golden, CO, 2020.

[17] NREL. ROSCO, 2022. URL: https://github.com/NREL/rosco.

[18] NREL. ROSCO toolbox, 2021. URL: https://github.com/NREL/ROSCO_toolbox/tree/main/Matlab_Toolbox/Simulink.

[19] C. Allen et al. Definition of the UMaine VolturnUS-S reference platform developed for the IEA wind 15-MegaWatt offshore reference wind turbine. Technical report, NREL, Golden, CO (US), 2020.

[20] M.Y. Mahfouz et al. Public design and FAST models of the two 15 MW floater-turbine concepts, 2020.

[21] J. G. Ziegler, N. B. Nichols, et al. Optimum settings for automatic controllers. *trans. ASME*, 64(11), 1942.

[22] IEC 61400-3-1:2019 - Wind energy generation systems - Part 3-1: Design Requirements for fixed offshore wind turbines. Technical report, British Standards Institution, London, UK, September 2019.

[23] F. Guo et al. Updates on the OpenFAST Lidar simulator. In *Journal of Physics: Conference Series*, volume 2265, page 042030. IOP Publishing, 2022.

[24] A. Jacobsen and M. Godvik. Influence of wakes and atmospheric stability on the floater responses of the hywind scotland wind turbines. *Wind Energy*, 24(2):149–161, 2021.